Impact of agricultural water-saving practices on regional evapotranspiration: The role of groundwater in sustainable agriculture in arid and semi-arid areas

Hang Chen[a], Zailin Huo[a,*], Xiaoqin Dai[b], Suying Ma[c], Xu Xu[a], Guanhua Huang[a]

[a] Centre for Agricultural Water Research in China, China Agricultural University, Beijing, 100083, PR China
[b] Qianyanzhou Ecological Station, Key Laboratory of Ecosystem Network Observation and Modeling, Institute of Geographic Sciences and Natural Resources Research, Chinese Academy of Sciences, Beijing, 100101, PR China
[c] Hebei Institute of Water Resources, Shijiazhuang, 055057, PR China

ARTICLE INFO

ABSTRACT

Evapotranspiration (*ET*) is an important component of the water budget process and is characterized by complex spatiotemporal changes, especially in irrigated agricultural areas. The impact of various hydrological processes and human activities on *ET* is still a meaty theme to study and investigate. A typical agricultural irrigation district with shallow groundwater and arid climate conditions was selected as the case study area in this work. The impact of the supplied irrigation water, shallow groundwater, crop planting pattern, and weather conditions on regional *ET* was determined after the regional *ET* was estimated by a Surface Energy Balance Algorithm of Land (SEBAL) model with Moderate Resolution Imaging Spectroratiometer (MODIS) data. The results show that the regional *ET* in Hetao kept declining in the past 15 years. The positive correlation between the water input (water diversion and precipitation) and *ET* indicated that reduced water diversion controls the declining *ET*, also causing the drop of groundwater level. Due to capillary forces and root uptake, the shallow groundwater tended to move upward to support the crop water consumption because the soil suffered from a water deficit. Furthermore, we quantified the contribution of shallow groundwater to regional *ET* and found that the water supplied from shallow groundwater increased from 5% to 15% during the period of water–saving irrigation. However, the long–term decrease of irrigation water supply and groundwater level caused a soil water deficit over the crop growth period, and the variation of crop planting pattern reduced *ET* as well. Therefore, groundwater plays an important role in sustainable agricultural development in arid and semiarid areas and the contribution of shallow groundwater to regional water consumption cannot be neglected.

1. Introduction

Evapotranspiration (*ET*) is an important part of regional or watershed water budgets. Understanding the spatial and temporal *ET* change is foundation for regional water resource management, especially in arid and semiarid areas. However, assessing the *ET* change in agricultural irrigation areas is still a huge challenge due to complex water cycle processes driven by irrigation and shallow groundwater. On one hand, traditional irrigation strategies have been improved by application of water-saving measures (WSM) for sustainable water use in arid and semiarid areas worldwide to cope with the water shortage in agricultural development (Zhang et al., 2011). On the other hand, excessive agricultural water-saving will cause the groundwater to decline

because the implementation of WSM is primarily responsible for the reduction of the seepage losses of irrigation water (Zhang et al., 2012). Supplied irrigation water will directly change the soil water deficit and induce a field *ET* change (Fig. 1). When the shallow groundwater is supplied from the infiltration of large amount of irrigation, less groundwater is consumed by evaporation because of the sufficient soil water. When the soil water deficit caused by a decreasing water supply negatively influences the regional *ET*, more of shallow groundwater moves upward to support the crop water consumption. Previous studies have proven that groundwater plays an important role in compensating for the high water consumption (*ET*) and the reduction of *ET* can be attributed to the decline of groundwater level (Liu et al., 2016; Balugani et al., 2017; Gao et al., 2017a, b; Jiang et al., 2017; Ramos et al., 2017;
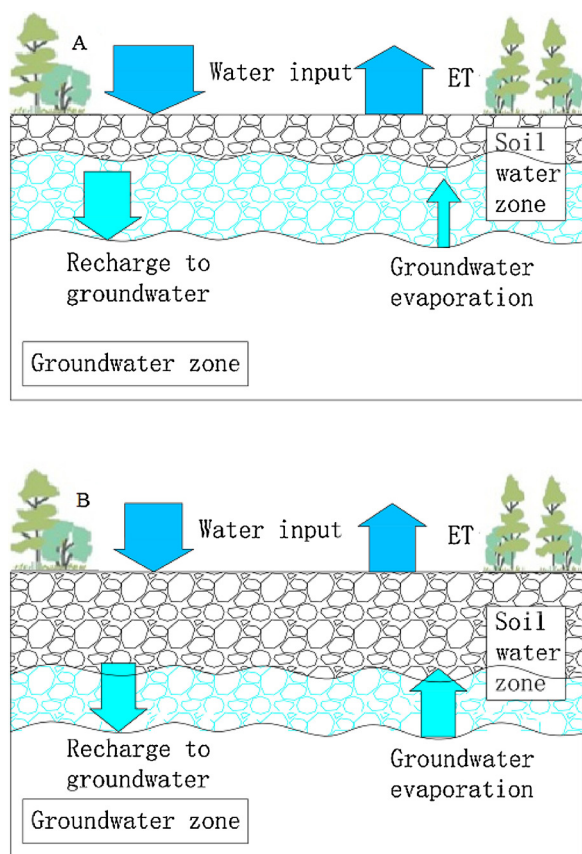
Fig. 1. Water cycle between surface water and groundwater.

Satchithanantham et al., 2017; Wang et al., 2016; Yang et al., 2017a, b). Both the WSM and groundwater decrease will therefore affect the *ET*.

Many studies focused on the impact of water-saving irrigation and groundwater on *ET*. By designing irrigation levels according to soil water content as a percentage of field capacity, Ran et al. (2017) found that *ET* under irrigation amount being 60%–55% and 50%–45% of field capacity decreased by 14% and 28.1% respectively, compared with *ET* under irrigation level of 70%–65%. Based on the application of WSM, the mean annual *ET* decreased from 752 mm to 610 mm in the North China Plain (Pei et al., 2017). Meanwhile, the soil water storage decreases with decreasing water input and groundwater level (Zdenek et al., 2017; Greaves and Wang, 2017; Alrajhi et al., 2017; Kisekka et al., 2017). As the shallow groundwater declined excessively, water deficit-induced stress negatively affected *ET* (Luo and Sophocleous, 2010). By conducting field experiments with different water treatments, Kirnak et al. (2002) observed that the soil water remained higher during full irrigation treatment and experienced less stress than using deficit irrigation. Based on a long–term field observation data, Liu et al. (2016) found that the soil moisture decreased significantly as the groundwater depth increased from near the ground surface to 2.5 m below the surface. Gao et al. (2017a, b) reached similar results using a process-based model.

Compared with scare surface water resources, shallow groundwater is essential for the maintenance of the high *ET* in arid and semiarid areas (Sepaskhah et al., 2003; Namuburg et al., 2005; Ghamarnia et al., 2013; Wang et al., 2014a; Wang et al., 2016). Previous studies confirm that the capillary upward movement of shallow groundwater by soil suction and root uptake can meet the water deficit when the soil moisture is insufficient to meet the crop water demand (Xue et al., 2017; Jorenush and Sepaskhah, 2003; Shouse et al., 2010; Wang et al., 2016). Soppe and Ayars (2003) showed that 40% of the daily crop

water use originated from groundwater on the west side of the San Joaquin Valley with shallow groundwater (< 1.5 m). Coincidentally, Cohen et al. (2006) proved that groundwater–supported *ET* accountd for as much as 12% of the total *ET* in a watershed of Minnesota. In addition to the irrigation water and groundwater, the long–term regional *ET* change also depends on the variation of the crop pattern considering the fact that the water consumption varies depending on the crop variety (Yang et al., 2017c; Yang et al., 2018; Bai et al., 2017).

Note that previous research about the influences on *ET* highly depending on field observations was limited to point or field scales (Kang et al., 2003; González–Altozano et al., 2008; Zhang et al., 2008; Zeppel et al., 2009; Wylie, 2003). Recently, the development of remote sensing techniques (RS) provided an effective way to understanding *ET* change at the regional scale. Based on the surface energy balance equation, the Surface Energy Balance Algorithm of Land (SEBAL) model has been successfully tested, it performs well with respect to in *situ* measurements and catchment hydrologic models in many regions (Allen et al., 2007; Li et al., 2008; Chang et al., 2017; Bastiaanssen et al., 2005; Lee and Kim, 2016; Bala et al., 2015; Bastiaanssen et al., 2010). Various RS–based–*ET* models have been developed over the past decades to study *ET* (Mu et al., 2011; Miralles et al., 2011; Norman et al., 1995).

To study the variation of *ET* and impact factors at a regional scale, the SEBAL model has been applied to estimate the *ET* in a typical irrigation district over the past 15 years. The main objectives of this study are: (1) to clarify the spatial and temporal variation of *ET* under water–saving irrigation conditions, (2) to assess the variation of the groundwater contribution to *ET*, and (3) to evaluate the long–term soil water deficit at the regional scale.

2. Material and methods

2.1. Study area

The Hetao Irrigation District (HID), located in the upstream part of the Yellow River Basin in China was selected as the study area. With a total area of $11.2 \times 10^3 \, \text{km}^2$, the HID is the third largest irrigation district in China (Wu et al., 2017) and includes five irrigation subdistricts: Yigan Irrigation District (YGID), Jiefangzha Irrigation District (JID), Yongji Irrigation District (YJID), Yichang Irrigation District (YCID) and Wulate Irrigation District (WID) (Fig. 2). The YGID is surrounded by the Gobi Desert and includes only one third of farmland. The farmland of the other four irrigation districts accounts for 60% of the total land area.
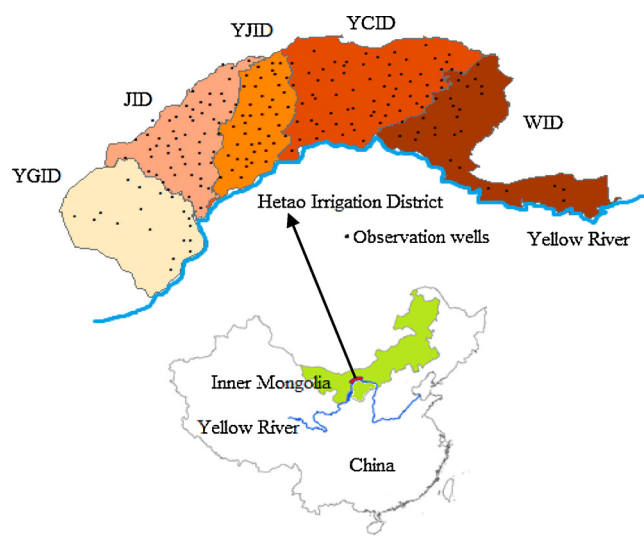
Fig. 2. Location of the study area (the solid black points reflect the distribution of the observation wells).

Table 1
Summary of the hydro–meteorological characteristics of the five subdistricts, including potential evaporation (E_0), mean annual precipitation (P), mean annual temperature (T), mean annual water diversion (I), total area (A) and irrigation area (A_i).

Subdistrict	E_0 (mm)	P (mm)	T (°C)	I (mm)	A (km²)	A_i (km²)
YGID	2680.54	139.83	9.24	355.69	2197.87	585.20
JID	1985.34	143.37	8.24	656.86	2156.80	1421.00
YJID	2226.29	139.99	9.24	664.05	1759.00	1167.47
YCID	2179.29	178.24	8.46	469.60	3138.07	1708.93
WID	2271.49	238.63	9.02	447.65	1424.33	805.53

The study area is located in an arid and semiarid continental climate zone with an average annual precipitation of ~170 mm and annual pan evaporation of ~2300 mm. The average annual temperature is ~8.8 °C while the maximum and minimum are –12.3 °C in January and 23.8 °C in July, respectively (Table 1). Most of the area of the HID is occupied by a plain with a slope of ~0.02%. Based on the estimated small Darcy velocity (~0.002 cm/day), the rapid horizontal groundwater flow is negligible. The vertical flux exchange is the main characteristic of shallow groundwater (Yu et al., 2010; Xu et al., 2010), including the infiltration of water, groundwater capillary uptake for *ET* and discharge through lateral drainage ditches.

As an important food base of China, the main crop in the HID includes spring maize, spring wheat, and sunflowers. Irrigation events are essential for agriculture production due to the arid climate and the main irrigation water is diverted from the Yellow River (Xu et al., 2010; Chen et al., 2016). The mean annual water diversion from the Yellow River to meet the agriculture irrigation is ~5.2 billion m³ (1980–2015), accounting for 10% of the total discharge of the Yellow River. The shallow groundwater produced by the large amount of water diversion varies from 0.5 to 2.5 m beneath the soil surface within a year.

With the increasing economic development, the water resource requirements for industrial and domestic use increase in the HID, similar to other developing regions. As a result, the allocated water resources for agricultural irrigation have been cut down (Zhang et al., 2011; Fu et al., 2007). A program identified by the Yellow River Conservancy Commission has been adopted in the HID since 1998 to resolve the issue of water shortage, reduce the water diversion from the Yellow River while maintaining the agricultural production. Multiple water–saving measures, including a reduction of water diversion, and lining of main canals, have therefore been applied to decrease the delivery losses and improve the irrigation water use efficiency.

2.2. Data collection

2.2.1. MODIS datasets for the SEBAL model

The *ET* distribution of the study area during 2000–2014 was calculated with the SEBAL method and available MODIS data. The datasets including MOD11A2, MOD13A2, MOD15A2, and MCD43B3 were downloaded from the NASA Data Center (https://reverb.echo.nasa.gov). The spatial resolution of the data is 1000 m and the temporal resolution of MOD11A2, MOD15A2 and MCD43B3 is 8d, while that of MOD13A2 is 16d. All original images were pre–projected in a Universal Transverse Mercator (UTM) projection. The Digital Elevation Model data with a spatial resolution of 90 m were downloaded from http://srtm.csi.cgiar.org/. Land use map was provided by Bayannur Survey and Design Institute of Water Conservancy and Hydropower.

2.2.2. Groundwater depth

A total of 228 observation wells were installed in the five subdistricts to monitor the groundwater depth every five days, that is, on days 6, 11, 16, 21, and 26 every month from 2000 to 2014. The mean monthly depth is the average of the five observation data points. The locations of the observation wells are shown in Fig. 2.

2.2.3. Irrigation, drainage and climate data

To support the agricultural production, irrigation water was diverted from the Yellow River from April to November every year. Monthly data of pan evaporation (2000–2014), precipitation (2000–2014), irrigation water (2000–2014), and annual drainage water data (2000–2014) in the five irrigration subdistricts were monitored and provided by the Hetao Irrigation District Administration. By assuming that the amount of drainage is dependent on water supply, the monthly drainage was estimated as:

$$Dr_i = \frac{I_i + P_i}{T(I + P)} \times TDr \tag{1}$$

where Dr_i, $I_i + P_i$ are the drainage and water supply over period i, (mm); $T(Dr)$ and $T(I + P)$ are the total amount of annual drainage and water supply, (mm). Irrigation water and precipitation constitute the total water input ($I + P$) of the whole district. In addition, daily flow data of the main canal systems of the JID from 2006 to 2013 were available.

2.2.4. Soil water content

Among the 56 groundwater observation wells in the JID, 22 wells were able to monitor the soil moisture by drying method before each irrigation event at the same intervals during 2006–2013. The soil profile in 1 m below surface was divided into five layers (0–10 cm, 10–20 cm, 20–40 cm, 40–70 cm, and 70–100 cm) and soil samples were drilled in each layer. The soil layers between 1 m and the groundwater level were regarded as the capillary water zone with high soil moisture, the variation of which was supposed to be negligible. The monthly soil moisture was estimated from the weighted average value of the five layers.

2.2.5. Crop planting area

The planting area data of various vegetation, including maize, wheat, and sunflowers in the five subdistricts from 2000 to 2014, was provided by the Hetao Irrigation District Administration. The variation of the crop pattern was determined by the planting ratio of each crop.

2.3. Methods

2.3.1. SEBAL model for the estimation of regional ET

The SEBAL model, which has been used since 1998, can estimate the daily *ET* based on remote sensing technology. Based on the surface energy balance equation, the *ET* is computed as energy residual (Bastiaanssen et al., 1998),

$$ET = \frac{R_n - G - H}{\lambda} \tag{2}$$

where *ET* is the estimated evapotranspiration, (mm); R_n, G, and H are the net radiation, soil heat flux and sensible heat (W/m^2), respectively, and λ is the latent heat of the evaporation of water (J/kg).

By converting the difference between the aerodynamic temperature and air temperature ($T_{Aero} - T_a$) into a linear relationship of the land surface temperature (T_s), the sensible heat (H) can be estimated as:

$$H = \frac{\rho C_p (T_{Aero} - T_a)}{r_a} = \frac{\rho C_p (aT_s + b)}{r_a} \tag{3}$$

where ρ is the air density, (kg/m^2); C_p is the specific heat capacity of air, ($J/kg \cdot °C$). The coefficient a and b can be defined by hot pixel and cold pixel. Due to the existence of Ulansuhai Lake, the cold pixel generally determined as a pixel with minimum temperature was always located in water body pixels, consistent with the selection criteria of traditional SEBAL model (Bastiaanssen et al., 2005). As to the hot pixels, the land use map, *NDVI* and T_s values (derived from MODIS dataset) were taken into account. After removing the pixels with small *NDVI* values (always less than 0.1) and extremely high temperature, the pixel having both high temperature and low *NDVI* values among the remaining candidate pixels (i.e. bare agricultural field determined by land use map) was

selected as the hot pixel. The detailed process can be referred to Allen et al. (2013) and Bhattarai et al. (2017).

r_a is the aerodynamic resistance to heat transport (s/m):

$$r_a = \frac{ln(z_2/z_1)}{u_* k} \tag{4}$$

where k is von Karman's constant of 0.41; $z_1 = 0.01$ m and $z_2 = 2$ m (Chandrapala and Wimalasuriya, 2003; Gieske and Merjninger, 2005; Singh et al., 2008). In fact, an alternative value of 0.1 for z_1 is also used in many papers (Chang et al., 2017; Mkhwanazi et al., 2015; Wang et al., 2014b). By conducting SEBAL model with four values of z_1, Paul et al. (2014) found that $z_1 = 0.01$ m and $z_1 = 0.1$ m led to the same estimate of ET (the comparison of ET values in this study and detailed information is shown in Fig. S1). u_* is the friction velocity (m/s):

$$u_* = \frac{k u_{200}}{ln(200/Z_{om})} \tag{5}$$

where u_{200} is the wind speed at the blending height of 200 m, converted from the wind velocity at a height of 2 m by the logarithmic wind law and z_{om} is the momentum roughness length (m):

$$z_{om} = 0.018 \times LAI \tag{6}$$

where LAI is the leaf area index.

For the stability examination of u_* and r_a, please refer to the studies of Paulson (1970) and Webb (1970).

Based on the above–mentioned SEBAL model, the ET estimated by Eq. (2) is an instantaneous value (ET_i, mm/s), which needs to be up-scaled to daily values (ET_d, mm/d) using the empirical formula (Jackson et al., 1983),

$$ET_d = 3600 \times \frac{2N(ET_i)}{\pi \sin(\pi t/N)} \tag{7}$$

where t is the difference between the time of sunrise and satellite passing; and N is the sunshine duration.

Because the MODIS datasets are collected and composited under cloudless sky conditions (the data of cloud affected pixels is blank), the estimated ET is supposed to be higher than the true value (Jia et al., 2012; van Leeuwen et al., 1999; Xiong et al., 2010). Considering the weather conditions, the total cloud cover (a proportion of the sky obscured by all clouds) was introduced to calibrate the ET during cloudy weather:

$$ET_{cloud} = a(f_{cloud} - 2)ET_{clear} \tag{8}$$

where f_{cloud} is the total cloud cover (0–10); ($f_{cloud} - 2$) means the impact of cloud (a clear sky is defined as less than 20 percent of cloud); and a is the cloud adjustment coefficient, that is, a constant of 0.132 after calibration. The monthly data of f_{cloud} is referred to Dabuxilatu Su and Deng (2009).

By averaging all available pixels of each subdistrict, we can obtain the daily ET value at an interval of 16d, that is, a total of 12 estimates during the crop growth period (at Day 97, 113…257 and 273 of a year). The ET estimated by the SEBAL model was regarded as the average of each 16-day period. The monthly data (monthly products are composited by calendar month) was based on the time-weighted average of the two to three 16-day SEBAL ET that contribute to each month; the monthly data was then accumulated into annual values.

2.3.2. Performance evaluation of the SEBAL model

The water balance method was selected in the present study to estimate the actual ET and test the performance of the SEBAL model. Compared with other methods introduced by hydrologists and meteorologists, the traditional water balance method is still a good alternative for the estimation of the ET in a closed basin and has a solid theoretical background (Xu and Chen, 2005; Billah et al., 2015). The estimated ET for the 22 soil water observation wells in the JID during the crop growth period of 2006–2013 was compared with the SEBAL ET

values picked at the corresponding wells pixels. Considering local hydrogeology conditions, the water balance method including 22 wells during the crop growth period can be expressed as:

$$\Delta W_g + \Delta W_s = P + I - Dr - ET \tag{9}$$

where P is the local precipitation denoted by the average values of the JID (mm); I is the irrigation water estimated by the sum of daily flow data of the nearby canal systems, (mm); Dr is the drainage through the drain ditches (mm); ET is the estimated evapotranspiration (mm); and ΔW_g and ΔW_g represent the storage variation of groundwater and soil water (mm),

$$\Delta W_g = \mu \times \Delta H \tag{10}$$

$$\Delta W_s = G \times \Delta S \times 1000 \tag{11}$$

where ΔH is the change of the groundwater depth, (mm); μ is the specific yield (nondimensional) of 0.07 (Hao et al., 2013) indicating the volumetric fraction of water yielded by a given aquifer under gravity; G is the thickness of the soil layer (supposed to be 1 m herein); and ΔS is the variation of the soil moisture, (mm). The application of all parameters is limited to the crop growth period.

To evaluate the performance of SEBAL model at different time scales, the actual ET based on field experiments in the HID was obtained from previous studies. Dai et al. (2011) measured the daily ET during crop growth period of 2009 in the Dengkou Agricultural Experiment Station by water balance method. Daily ET were aggregated to 16–day ET with the same durations of SEBAL ET to conduct validation. In addition, the actual ET measured by the Bowen ratio system at same durations in 2014 of the YJID was provided by the Fenzidi Experiment Station. The monthly ET of 2006–2008 in the YCID are referred to Jia et al. (2013) and Wu et al. (2006).

The MOD16 A2 Evapotranspiration products of 2000–2014 (MOD ET for short) with spatial-temporal resolution of 1000 m and 8d were selected to conduct model intercomparison as well. The detailed information about MOD16 algorithm is referred to Mu et al., 2007.

2.3.3. Contribution of shallow groundwater to ET

In our previous research (Chen et al., 2016), we observed that the groundwater depth change in the HID with a declining trend during the crop growth period can be attributed to the abundant water consumption for ET. Thus, the groundwater net consumption (ET_{ng}) during the crop growth period can be estimated as follows:

$$ET_{ng} = \Delta W_g - D_r = \mu \times \Delta H - Dr \tag{12}$$

where μ and ΔH are the same parameters as Eq. (10); Dr is the drainage in the same period, (mm). The contribution of groundwater to ET was determined as the ratio of ET_{ng} to ET (ET_{ng}/ET) (Cohen et al., 2006; Chen et al., 2016; Gao et al., 2017a,b).

2.3.4. Estimation of the regional soil water deficit

The soil moisture is the main factor restricting ET in arid and semiarid areas. In this study, we used the soil water deficit as the term determining the soil water conditions. Usually, we can estimate the field ET using the FAO equation, wherein the ET is the product of the crop coefficient, soil water coefficient and reference evaporation (Allen et al., 1998). Furthermore, the soil water deficit factor is determined based on irrigation and groundwater levels.

Based on the evaporation proportional hypothesis (Penman, 1948) and FAO 56, the estimation of field ET can be expressed as:

$$ET = K_S \times K_C \times ET_0 \tag{13}$$

where K_S and K_C are the water stress and crop coefficient (non–dimensional), reflecting the impact of soil moisture deficit and crop growth conditions, respectively. The reference evaporation ET_0 can be converted from the pan evaporation E_0 by multiplied by a constant coefficient of 0.55 (Ren et al., 2002):
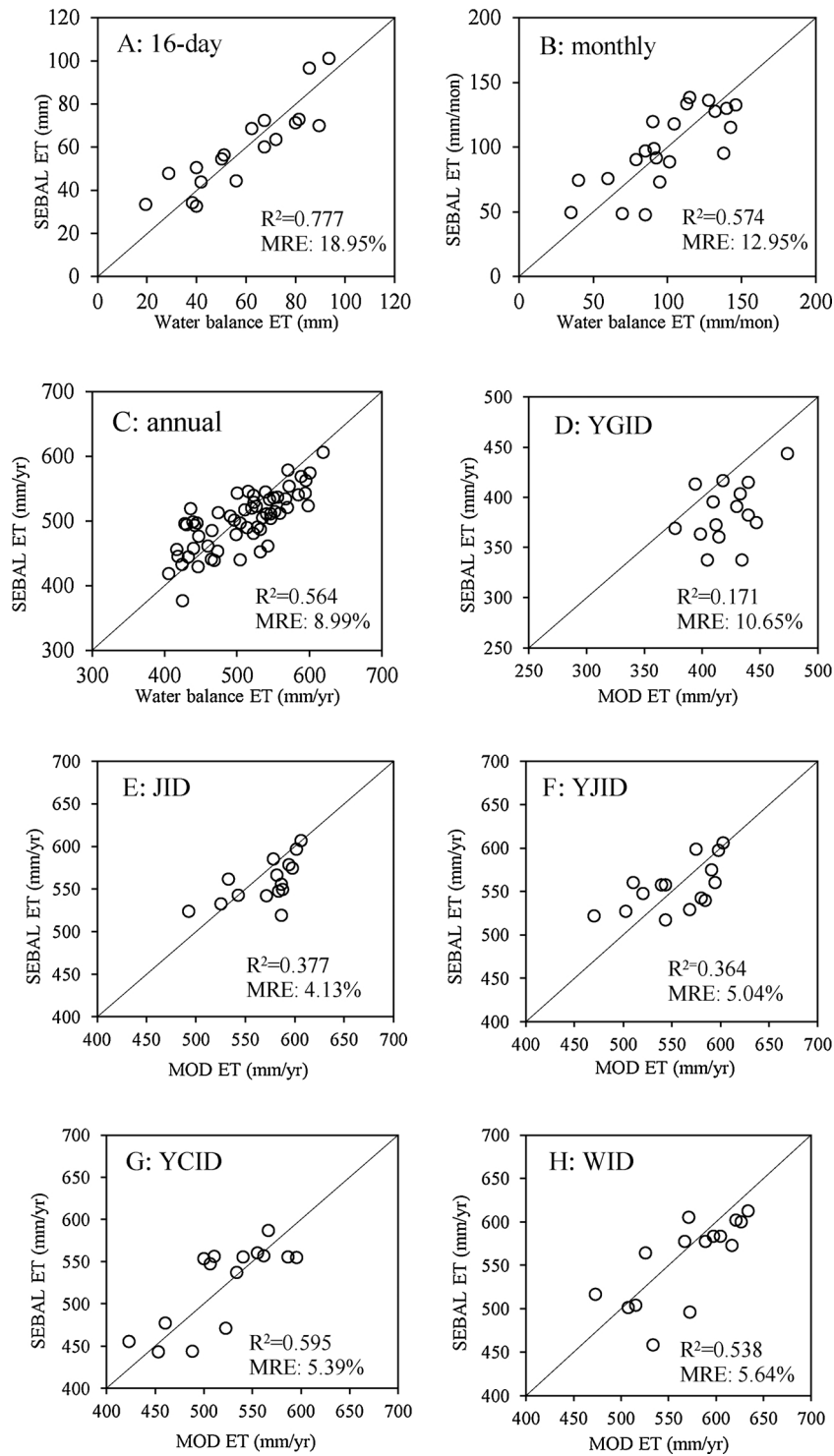
Fig. 3. A–C: Comparison between the SEBAL *ET* and actual *ET* at different time scales in the HID; D–H: Intercomparison between SEBAL model and MOD16 product.

$$ET_0 = 0.55 \times E_0 \tag{14}$$

Here, we extended Eq. (13) to the regional scale. For the regional scale, the crop coefficient K_C reflecting the variation of the vegetation growth depending on the main crop pattern (wheat, maize, and sunflowers, etc.) and stage duration of each crop growth period (initial, rapid growth, middle, and late). In each subdistrict, the local K_C was estimated by the weighted average as:

$$K_C = \sum \left(\sum K_{Cij} L_{ij} \right) \times A_i \tag{15}$$

where K_{Cij} is the crop coefficient at a different growth stage; L_{ij} is the ratio of each stage duration to the total crop growth period; i = kinds of vegetation; j = initial, rapid growth, middle, and late growth period; and A_i is the planting area ratio of crop i, estimated as the planting area of each crop divided by the total planting area. The estimation of K_S can then be expressed as follows:

$$K_S = \frac{ET/ET_0}{K_C} \tag{16}$$
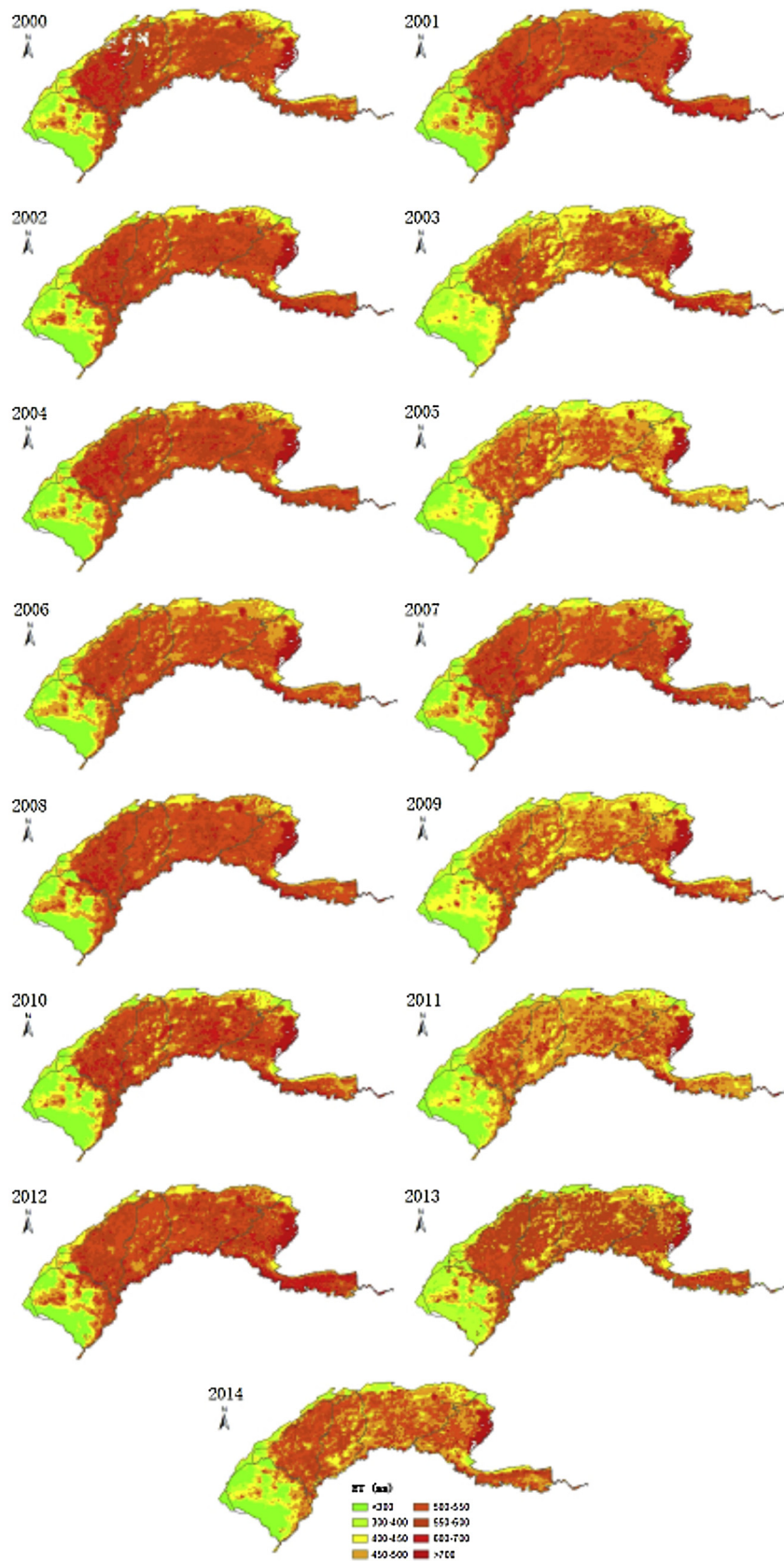
Fig. 4. Spatial distribution of the total *ET* in the HID from 2000 to 2014.
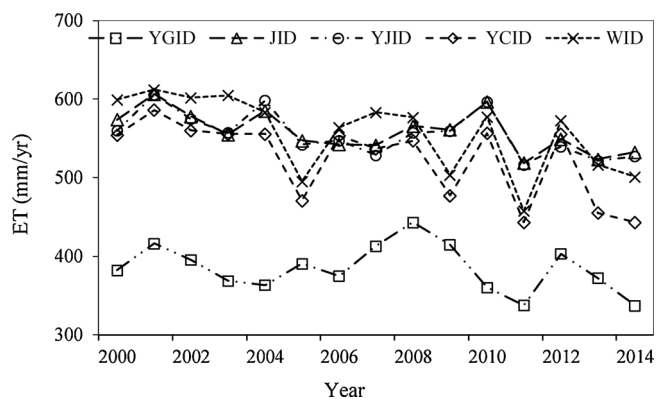
Fig. 5. Variation of the mean annual *ET* in five subdistricts.from 2000 to 2014.

3. Results

3.1. SEBAL model validation

As shown in Fig. 3A–C, the mean relative errors (MREs) at different scales show that the SEBAL model has a higher precision in evaluating the annual–scale *ET* (crop growth period in present study) than the monthly– and 16–day– scale values. The MRE at the annual scale was 8.99%, while that at monthly and 16–day scales reached up to 12.95% and 18.95%, respectively. The results are in accordance with the previous study. Based on the estimation of the annual *ET* in Sri Lanka, Bastiaanssen and Chandrapala (2003) reported that the MRE of the SEBAL model in the regional field ranged from 1% to 11%, while Hemakumara et al. (2003) obtained a MRE on a 10–day basis ranging from 4% to 32%. In the present area, the SEBAL–estimated *ET* in the HID without WID was compared with the actual *ET* at regional scale by Yang et al. (2012). The MRE of the annual *ET* was 5.6%, which is similar to the results of this study.

The use of contaminated inputs of MOD16 will produce incorrect ET estimates (Kim et al., 2012). Due to the missing data of desert pixels, the accumulated MOD *ET* overestimated regional *ET* of the YGID while the estimates in the other four districts were in good agreement with SEBAL *ET* (Fig. 3D–H). Considering the fragment–cultivating pattern (means small field size) in the study area, the accuracy of the SEBAL model meets the precision requirements on the regional annual *ET*.

3.2. Temporal and spatial change of ET during the past 15 years

Based on the Geographic Information System (GIS), the regional *ET* derived from the SEBAL method can clearly describe the spatial variation of *ET* in the HID (Fig. 4). Note that the mean annual *ET* varied from 200 to 900 mm in the whole irrigation district under different land use patterns and water resource conditions. Due to the existence of the Gobi Deserts and shortage of water supply in the west of the HID, the annual *ET* in the YGID of ~388 mm was notably lower than that in the

other four districts (annual average of 552 mm). The highest *ET* was observed for the Ulansuhai Lake located in the WID. A higher *ET* was obtained in the JID and WID. The characteristics of spatial distribution has not changed significantly over the period of 2000–2014. The mean annual *ET* in 2005, 2009, 2011, 2013, and 2014 was significantly smaller than the multi–annual average of 515.8 mm/yr. The *ET* during the crop growth period showed a declining trend in the subdistricts during the past 15 years, except for the YGID. The decline of the *ET* in the JID and YJID was approximately 50 mm, while that in YCID and WID reached up to 100 mm (Fig. 5). The variation of the *ET* in the HID as an arid area with irrigated agricultural production can be attributed to the changes of the water supply and crop planting patterns. Details will be discussed in the following sections.

3.3. Impact of water input and shallow groundwater on the regional ET

Generally, the regional *ET* in the irrigation area is controlled by the combined influence of climate change (i.e., temperature and precipitation), water input, and shallow groundwater. Because of the stable temperature over crop growth period (Fig. S2A), the variation of temperature was supposed to have little impact on *ET*. Meanwhile, the actual *ET* in arid area was proven to be mainly limited by water amount (Yang et al., 2006; Han et al., 2014). So the water input and shallow groundwater are considered as the main influence factors on *ET* (the less precipitation is regarded as water supply, along with irrigation water). Based on the WSM, the annual water diversion for irrigation in the HID from 2000 to 2014 ha s been reduced by 20% to maintain the sustainable utilization of water resources. Fig. S2B in Appendix shows the significant decrease of the water input of the HID from 2000 to 2014. The *ET* variation pattern is similar to that of the water input in the HID. The positive relationship between the *ET* and water input indicates that the water amount is responsible for the *ET* change in study area (Fig. 6A). Similar to the results of Gao et al. (2017a,b), the mean *ET* during the crop growth period in the five subdistricts decreased from 543.9 to 498.3 mm when the water input decreased from 616.6 to 521.2 mm (Fig. 6B). The smaller decline of the *ET* compared with that of water input suggests that the shallow groundwater was consumed to support crop water requirements.

Based on the shallow groundwater depth and arid climate, groundwater evidently contributes to *ET* (Chen et al., 2016; Gao et al., 2017a,b; Liu et al., 2016; Wang et al., 2016). In the present study, 2003, 2006, 2010, and 2013 were selected as years with typical spatio-temporal groundwater depth characteristic (Fig. S3A in the Appendix). The mean annual groundwater depth in the northeast of the HID was shallower than that in the southwest, while the *ET* in the northeast was larger than that in southwest. With the application of WSM, the mean groundwater depth during the crop growth period in the HID increased from 1.78 m in 2000 to 2.15 m in 2014 (Fig. S3B listed in the Appendix) and the rate of groundwater level notably decreased from 2006 in response to the rising water diversion. Considered as a potential water resource for crop consumption, the decline of the shallow groundwater
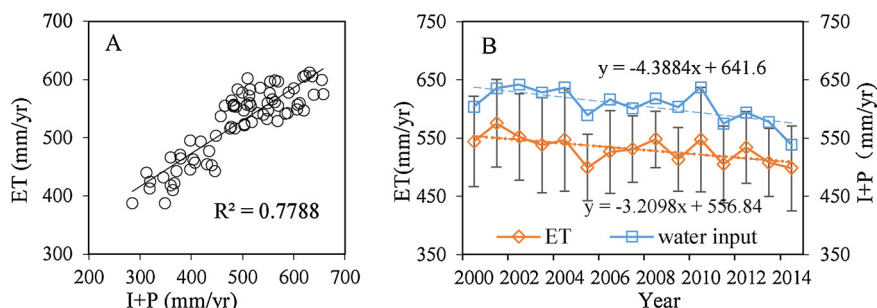
Fig. 6. A: Relationship between the *ET* and water input (*I* + *P*); B: Trends of the *ET* and water input (*I* + *P*) in the HID from 2000 to 2014 (the error lines indicate the upper and lower bounds of regional *ET* in the HID).
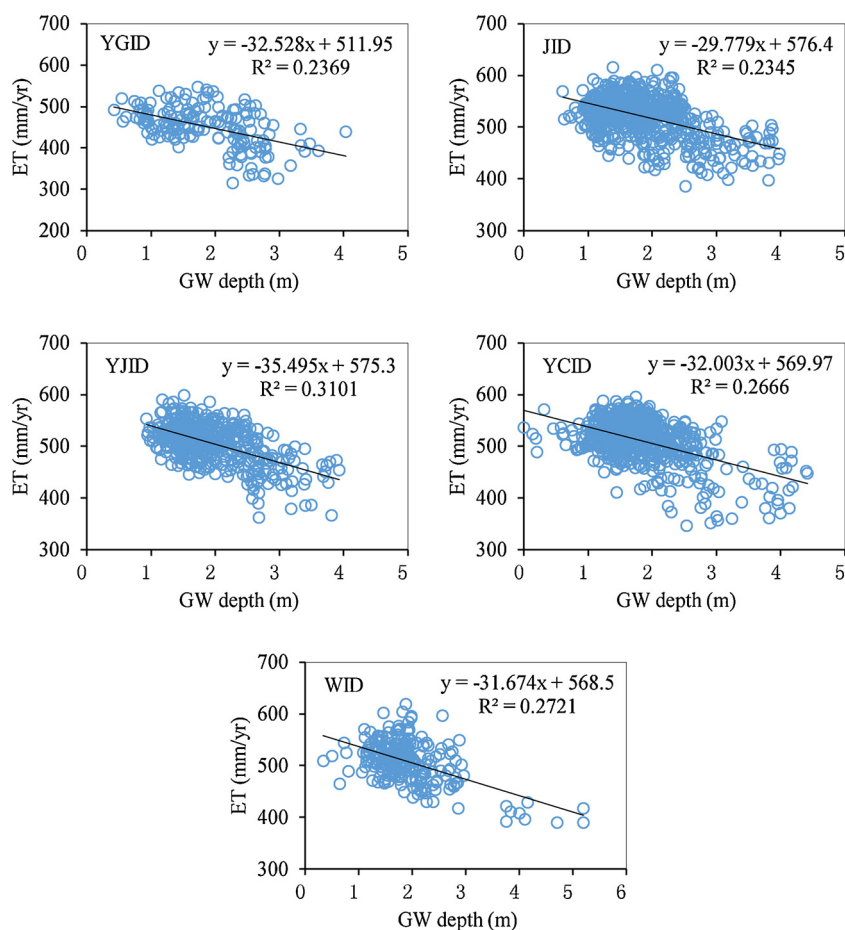
Fig. 7. Relationship between the *ET* and groundwater depth in the five subdistricts.

diminished the total water supply for regional *ET*. The positive relationship between the groundwater depths of 228 observation wells and *ET* values of corresponding pixels indicates that the *ET* was also impacted by the shallow groundwater (Fig. 7), which is consistent with the findings of previous studies (Huo et al., 2012a, b).

4. Discussion

4.1. Contribution of groundwater to ET

As a result of WSM, the contribution of groundwater to *ET* is assumed to vary depending on the combined impact of water supply and groundwater (Gao et al., 2017a,b; Chen et al., 2016; Liu et al., 2016). Compared with the declining tendency of the water input during 2000–2014, the contribution ratio of shallow groundwater to evaporation (ET_{ng}/ET) in the HID showed an increasing trend (Fig. 8A). Because of WSM, the maximum contribution ratio has increased from 5% to 15% during the past 15 years. The ET_{ng}/ET values using MOD *ET* were slightly less than that using SEBAL *ET* which can be attributed to the missing data in desert pixels of MOD16 products (Fig. S4). These results indicate that more shallow groundwater moved upward to cope with crop water requirements because less irrigation water was applied, which is in good agreement with the study of Luo and Sophocleous (2010).

Based on our results, water-saving irrigation can enhance the groundwater contribution to regional *ET* in the HID. However, according to water cycle processes, the shallow groundwater level declined with decreasing recharge from the infiltration of irrigation water and caused the decline of the groundwater contribution to *ET* (Ramos et al., 2017; Balugani et al., 2017; Karimov et al., 2014; Sepaskhah

et al., 2003). In contrast to previous research, we found that more groundwater contributed to *ET* although the groundwater level showed decline with decreasing irrigation water amount in the present study (Fig. 8B). Notably, compared with the linear relationship, the response of the ET_{ng}/ET ratio to the groundwater depth is characterized by a single-peak curve. We call the groundwater depth responding to the maximum ET_{ng}/ET ratio "critical groundwater depth (*GWDc*)". When the groundwater depth is smaller than the *GWDc*, the ET_{ng}/ET ratio increases with decreasing groundwater level. This increase of the ET_{ng}/ET ratio can be attributed to the larger effect of the soil water deficit compared with that of declining groundwater. However, when the groundwater depth is larger than the *GWDc*, the ET_{ng}/ET ratio decreases with decreasing groundwater levels (Fig. S5 listed in the Appendix). In the early study period, the abundant water diversion for irrigation in the HID resulted in high groundwater levels and enough soil water storage for crop water consumption. Therefore, less groundwater was consumed for *ET*, although the groundwater level was shallow. Subsequently, the decreasing water input induced the decline of the groundwater levels. At the same time, the soil water became more and more insufficient in supporting the crop water requirements, and shallow groundwater moved upward by capillary uptake to support *ET* (Ghamarnia et al., 2013; Karimov et al., 2014; Sepaskhah et al., 2003; Yang et al., 2007). Meanwhile, the increasing groundwater consumption and reduced water recharge accelerated the decline of the groundwater level. When the groundwater level declined to the *GWDc*, the water supplied from groundwater decreased and gradually vanished due to the weakened capillary force (Huo et al., 2012a, b; Steinwand et al., 2006).

Fig. 8B shows the ET_{ng}/ET variation of five subdistricts compared with the groundwater depth. In the YGID with deeper groundwater, the

A:
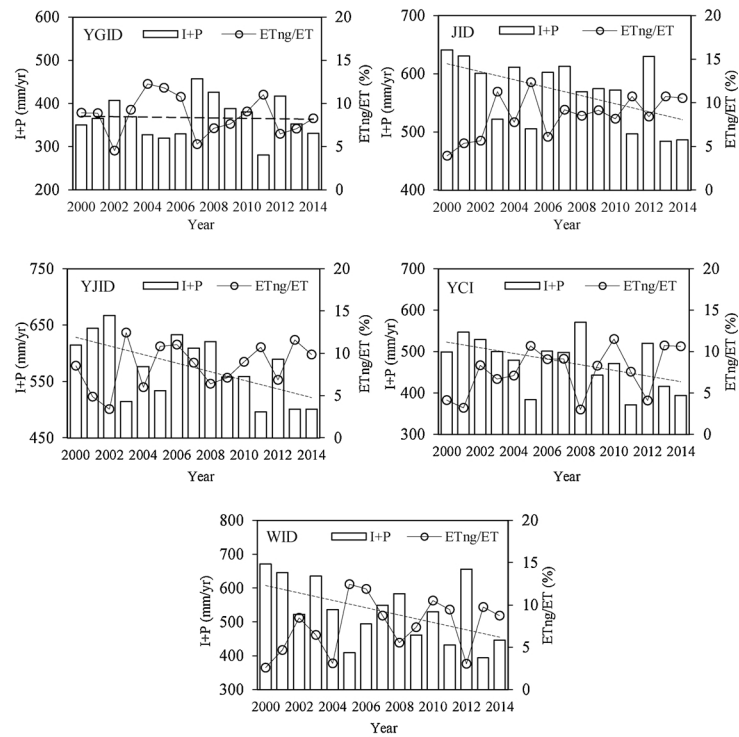
B:
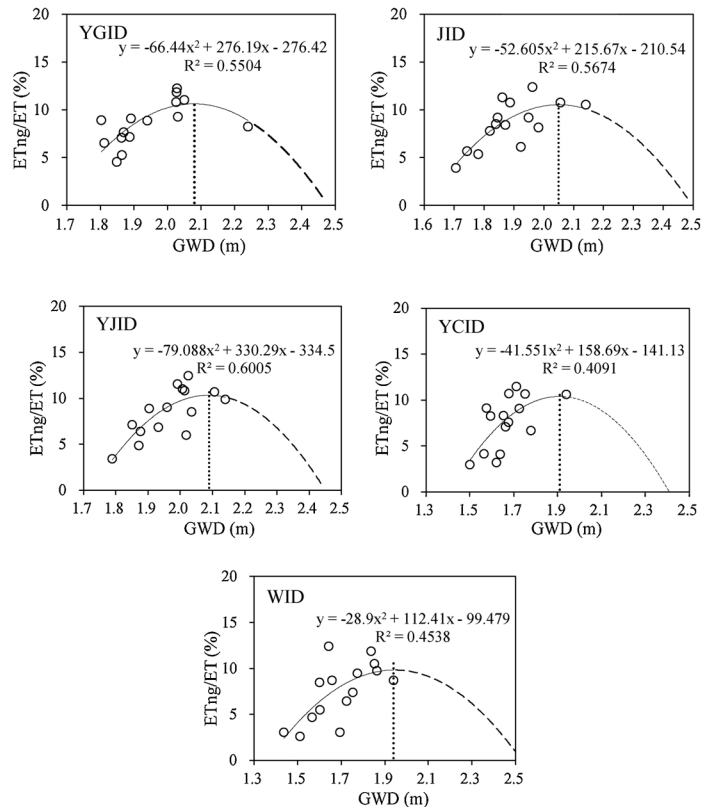
Fig. 8. A: Variation of the water input and groundwater net consumption; B: Relationship between the ET_{ng}/ET ratio and groundwater depth (the solid and dashed curves reflect the actual and predicted trends of the ET_{ng}/ET variation, respectively).

Table 2
Weighted average K_C of different crops during the whole crop growth period.

	wheat	maize	sunflower	oil plants	melons	tomato	forest	grassland
Initial	0.605	0.730	0.697	0.350	0.500	0.600	0.800	0.400
Rapid growing	0.946	0.982	0.751	0.735	0.735	0.858	0.980	0.784
Middle	1.286	1.118	0.804	1.150	1.000	1.150	1.200	1.200
Late	0.250	0.542	0.350	0.350	0.800	0.800	0.850	1.150
Weighted average	0.956	0.982	0.715	0.724	0.759	0.883	1.036	0.920

Note: Initial period lasts from early-mid April to late May; rapid growing period lasts from early June to mid-late July; middle period lasts from late July to late August or early September; late period lasts from early September to late September or early October.

A:

B:
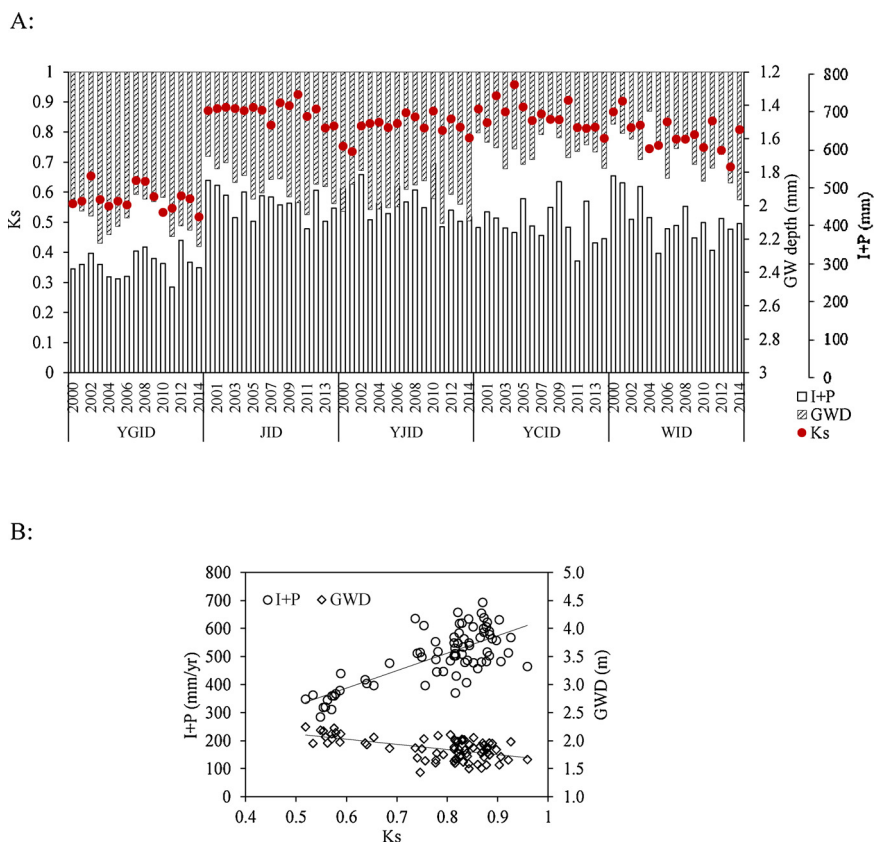
Fig. 9. A: Variation of the water input, groundwater depth, and K_S; B: Relationship between K_S and the groundwater depth and water input.from 2000 to 2014.

ET_{ng}/ET value started to decrease with increasing groundwater depth below 2.08 m. In the JID and YJID, the inflection point of the curves seemed to appear with increasing groundwater depth. In the YCID and WID with shallower groundwater depths, the ET_{ng}/ET values continuously increased with increasing groundwater depth, but the increase rate decreased. If the groundwater level keeps declining, the ET_{ng}/ET value is about to decrease as well. The variation of the ET_{ng}/ET values with groundwater depth in different subdistricts indicate that maintaining groundwater level in a reasonable range plays an important role in maintaining ecological balance in arid areas. It is worth to further study the rational water management for irrigation. In the HID, the mean critical groundwater depth was determined to be ~2.01 m.

4.2. Variation of the soil water deficit

The ET during the crop growth period was positively correlated with pan evaporation in the HID (Fig. S6 listed in the Appendix). To quantify the effect of irrigation on regional ET, we first calculated the conversion coefficient $K_C \times K_S$ based on the ratio of ET to ET_0. We then determined K_C using the crop planting pattern data and K_S from the evaporation

proportional equation. The parameters K_C and K_S were proven to vary with the crop pattern variation and soil water conditions (Scaini et al., 2015; Keshavarz et al., 2014; Ceppi et al., 2014).

The crop pattern in the HID has changed greatly from 2000 to 2014, affected by the agricultural product market and national economic policies (Fig. S7 in the Appendix). Based on the empirical crop coefficient at different stages in the HID by Dai et al. (2011), the weighted average K_C of each crop during the whole crop growth period is shown in Table 2. The maximum K_C value of the main crops was obtained for maize, followed by wheat and sunflowers. With the sharp increase of sunflowers and decrease of wheat, K_C of the five subdistricts showed a significant decrease (Fig. S8 in the Appendix). According to FAO–56, the decline of the K_C means that the crop will reduce the water consumption. We can extend this equation to the regional scale, where K_C is determined by the allocation of the crop pattern. In case of the present study, the K_C decrease in the five subdistricts will result in the decline of regional ET.

Fig. 9A shows that, the value of K_S in the YGID was clearly lower than that of the other four subdistricts due to the smaller amount of water diversion and arid climate conditions (existence of deserts). With lower water diversion but shallower groundwater depth, the value of K_S

in the YCID and WID was almost the same as that in the JID and YJID. This is likely related to the assumption that the variation of K_S is affected by the combined influence of water diversion and groundwater depth. The K_S variation in each subdistrict during 2000–2014 was divided into two domains, that is, before 2008 and after 2008. The parameter K_S remained high level before 2008, then kept declining. The significant relationship between K_S and the groundwater depth and water diversion confirms the above-mentioned hypothesis and provides the cause for the variation of K_S (Fig. 9B). In the early period of WSM application, the shallow groundwater can still contributed to support crop water consumption as the water diversion reduced. However, the continuous reduction of the groundwater without the resupply from water infiltration failed to meet soil deficit later and the crop became less resistant to water stress (Man et al., 2016; Ma et al., 2016; Zhang et al., 2017; Kögler and Söffker, 2017). The severity of water stress increases as the value of the coefficient deceases (Allen et al., 1998). The increasing water stress due to deficit irrigation has been proven to cause a significant decline in the crop water consumption (Greaves and Wang, 2017; Caser et al., 2017)

In the present study, the declining K_S value is an indicator of the soil drought caused by the shortage of the water supply, leading to a soil water deficit that limits the water available for crop growth. This result is consistent with previous research (Yang et al., 2017c; Panu and Sharma, 2002; Sepulcre–Canto et al., 2012; McWilliam, 1986; Seneviratne et al., 2010). Using satellite remote–sensing based soil moisture, Nicolai–Shaw et al. (2017) found that soil drought is relevant for reduced water supply and increased groundwater depth. Based on surveying 275 famers in Northeast United States, Sweet et al. (2017) showed that crop losses derived by soil deficit are attributed to an inadequate irrigation capacity and water supply. Moderate water stress induced by suitable WSM can promote the water use efficiency while maintaining the yield, but the severe water stress will have a serious negative impact on agriculture production (Torrion and Stougaard, 2017; Ceppi et al., 2014). The strong link between K_S and the water diversion and groundwater level further emphasizes the importance of rational water management in arid areas.

5. Conclusions

In this study, the SEBAL model with MODIS data performed well in estimating the *ET* of the HID of the past 15 years. Our results showed that the actual *ET* in arid areas was mainly controlled by the variability in water input and shallow groundwater. With the reduced water supply through diversion, the mean annual *ET* during the crop growth period in the HID during 2000–2014 decreased from 543.9 to 498.3 mm and the groundwater depth increased from 1.78 to 2.15 m. Meanwhile, the groundwater net consumption to *ET* (ET_{ng}/ET) continued to increase, indicating that more groundwater was used to meet the crop water demand. However, the soil drought and water deficit derived by the declined water input and groundwater level are worth to discuss. Shallow groundwater is a very important water resource to meet crop demands, especially in arid areas with agricultural irrigation. The application of proper water diversion management to keep the groundwater depth in a reasonable range is the primary focus of WSM. Overall, the role of groundwater in the sustainable development of regional agriculture needs to be considered when agricultural water–saving irrigation is put forward in arid and semiarid areas. In future studies, water cycle process–based analysis should be considered to quantify the contribution of groundwater to meeting the crop water requirements at the irrigation district scale.

Acknowledgements

Appendix A. Supplementary data

Supplementary material related to this article can be found, in the online version, at doi:https://doi.org/10.1016/j.agrformet.2018.08.013.

References

Allen, R.G., Pereira, L.S., Raes, D., Smith, M., 1998. Crop Evapotranspiration: Guidelines for Computing Crop Water Requirements FAO Irrigation and Drainage. Paper 56. Rome. .

Allen, R.G., Tasumi, M., Trezza, R., 2007. Satellite–based energy balance for mapping evapotranspiration with internalized calibration (METRIC)—model. J. Irrig. Drain. E 133, 380–394.

Allen, R.G., et al., 2013. Automated calibration of the METRIC-Landsat evapotranspiration process. J. Am. Water Resour. Assoc. 49, 563–576.

Alrajhi, A., Beecham, S., Hassanli, A., 2017. Effects of partial root–zone drying irrigation and water quality on soil physical and chemical properties. Agric. Water Manage. 182, 117–125.

Bai, L.L., Cai, J.B., Liu, Y., Chen, H., Zhang, B.Z., Huang, L.X., 2017. Responses of field evapotranspiration to the changes of cropping pattern and groundwater depth in large irrigation district of Yellow River basin. Agric. Water Manage. 188, 1–11.

Bala, A., Rawat, K.S., Misra, A.K., Srivastava, A., 2015. Assessment and validation of evapotranspiration using SEBAL algorithm and Lysimeter data of IARI agricultural farm. India. Geocarto Int. 31, 739–764.

Balugani, E., Lubczynski, M.W., Reyes-Acosta, L., 2017. Groundwater and unsaturated zone evaporation and transpiration in a semi–arid open woodland. J. Hydrol. 547, 54–66.

Bastiaanssen, W., Chandrapala, L., 2003. Water balance variability across Sri Lanka for assessing agricultural and environmental water use. Agric. Water Manage. 58, 171–192.

Bastiaanssen, W., Pelgrum, H., Wang, J., Ma, Y., Moreno, J.F., 1998. A remote sensing surface energy balance algorithm for land (SEBAL) 2. Validation. J. Hydrol. 212–213, 213–229.

Bastiaanssen, W., Noordman, E.J.M., Pelgrum, H., Davids, G., Thoreson, B.P., Allen, R.G., 2005. SEBAL model with remotely sensed data to improve water–resources management under actual field conditions. J. Irrig. Drain. Eng. 131, 85–93.

Bastiaanssen, W., Thoreson, B.P., Clark, B., Davids, G., 2010. Discussion of "Application of SEBAL Model for Mapping Evapotranspiration and estimating surface energy fluxes in South–Central Nebraska" by Ramesh K. Singh, Ayse Irmak, Suat Irmak, and Derrel L. Martin. J. Irrig. Drain. Eng. 136, 282–283.

Bhattarai, N., Quackenbush, L.J., Im, J., Shaw, S.B., 2017. A new optimized algorithm for automating endmember pixel selection in the SEBAL and METRIC models. Remote Sens. Environ. 196, 178–192.

Billah, M.M., Goodall, J.L., Narayan, U., Reager, J.T., Lakshmi, V., Famiglietti, J.S., 2015. A methodology for evaluating evapotranspiration estimates at the watershed–scale using GRACE. J. Hydrol. 523, 574–586.

Caser, M., Lovlsolo, C., Scarlot, V., 2017. The influence of water stress on growth, ecophysiology and ornamental quality of potted Primula vulgaris 'Heidy' plants. New insights to increase water use efficiency in plant production. Plant Growth Regul. 83, 361–373.

Ceppi, A., Ravazzani, G., Corbari, C., Salerno, R., Meucci, S., Mancini, M., 2014. Real–time drought forecasting system for irrigation management. Hrdrol. Earth. Syst. Sci. 18, 3353–3366.

Chandrapala, L., Wimalasuriya, M., 2003. Satellite measurements supplemented with meteorological data to operationally estimate evaporation in Sri Lanka. Agric. Water Manage. 58, 89–107.

Chang, Y.P., Ding, Y.J., Zhao, Q.D., Zhang, S.Q., 2017. Remote estimation of terrestrial evapotranspiration by Landsat 5 TM and the SEBAL model in cold and high–altitude regions: a case study of the upper reach of the Shule River Basin. China. Hydrol. Process. 31, 514–524.

Chen, H., Liu, Z.X., Huo, Z.L., Qu, Z.Y., Xia, Y.H., Fernald, A., 2016. Impacts of agricultural water saving practice on regional groundwater and water consumption in an arid region with shallow groundwater. Environ. Earth. Sci. 75. https://doi.org/10.1007/s12665–016–6006–6.

Cohen, D., Person, M., Daannen, R., Locke, S., Dahlstrom, D., Zabielski, V., 2006. Groundwater–supported evapotranspiration within glaciated watersheds under conditions of climate change. J. Hydrol. 320, 484–500.

Dabuxilatu Su, L.J., Deng, X.D., 2009. Spatial-temporal distribution and change trend of cloud amount over Inner Mongolia. Meteorol. Sci. Technol. (Chinese) 37, 306–310.

Dai, J.X., Shi, H.B., Tian, D.L., Xia, Y.H., Li, M.H., 2011. Determination of crop coefficients of main grain and oil crops in Inner Mongolia Hetao Irrigation area. Irri. Drain. 30, 23–27.

Fu, G., Charles, S.P., Viney, N.R., Chen, S., Wu, J.Q., 2007. Impacts of climate variability on stream–flow in the Yellow River. Hydrol. Process. 21, 3431–3439.

Gao, X.Y., et al., 2017a. Deficit irrigation enhances contribution of shallow groundwater to crop water consumption in arid area. Agric. Water Manage. 185, 116–125.

Gao, X.Y., Huo, Z.L., Qu, Z.Y., Xu, X., Huang, G.H., Steenhuis, T.S., 2017b. Modeling contribution of shallow groundwater to evapotranspiration and yield of maize in an arid area. Sci. Rep. 7. https://doi.org/10.1038/srep43122.

Ghamarnia, H., Golamian, M., Sepehri, S., Arji, I., Norozpour, S., 2013. The contribution of shallow groundwater by safflower (Carthamus tinctorius L.) under high water table conditions, with and without supplementary irrigation. Irrig. Sci. 31, 285–299.

Gieske, A., Merjninger, W., 2005. High density NOAA time series of ET in the Gediz Basin. Turkey. Irrig. Drain Syst. 19, 285–299.

González–Altozano, P., Pavel, E.W., Oncins, J.A., Doltra, J., Cohen, M., Paco, T., Massai, R., Castel, J.R., 2008. Comparative assessment of five methods of determining sap flow in peach trees. Agric. Water Manage. 95, 503–515.

Greaves, G.E., Wang, Y.M., 2017. Effect of regulated deficit irrigation scheduling on water use of corn in southern Taiwan tropical environment. Agric. Water Manage. 188, 115–125.

Han, S.J., Tian, F.Q., Hu, H.P., 2014. Positive or negative correlation between actual and potential evaporation? Evaluating using a nonlinear complementary relationship model. Water Resour. Res. 50, 1322–1336.

Hao, F.H., Sun, M.Z., Zhang, X., OuYang, W., Guo, B.B., Huang, H.B., 2013. Dynamic of soil water, groundwater and water balance in Hetao Irrigation Area. Acta. Sci. Circumst. 33, 771–779.

Hemakumara, H.M., Chandrapala, L., Moene, A.F., 2003. Evapotranspiration fluxes over mixed vegetation areas measured from large aperture scintillometer. Agric. Water Manage. 58, 109–122.

Huo, Z.L., Feng, S.Y., Huang, G.H., Zheng, Y.Y., Wang, Y.H., Guo, P., 2012a. Effect of groundwater level depth and irrigation amount on water fluxes at the groundwater table and water use of wheat. Irrig. Drain. 61, 348–356.

Huo, Z.L., Feng, S.Y., Dai, X., Zheng, Y.Y., Wang, Y.H., 2012b. Simulation of hydrology following various volumes of irrigation to soil with different depths to the water table. Soil. Use. Manage. 28, 229–239.

Jackson, R.D., Hatfield, J.L., Reginato, R.J., Idso, S.B., Pinter, P.J., 1983. Estimation of daily evapotranspiration from one time–of–day measurements. Agric. Water Manage. 7, 351–362.

Jia, Z.Z., Liu, S.M., Xu, Z.W., Chen, Y.J., Zhu, M.J., 2012. Validation of remotely sensed evapotranspiration over the Hai River Basin. China. J. Geophys. Res. Atmos. 117. https://doi.org/10.1029/2011JD017037.

Jia, S., Yue, W.F., Wang, J.S., Gao, H., Chen, A.P., 2013. Groundwater balance in the Yichang Irrigation District in Inner Mongolia in the past 20 years. J. Beijing Normal Univ. (Nat. Sci.) 49, 243–245.

Jiang, X.W., Sun, Z.C., Zhao, K.Y., Shi, F.S., Wan, L., Wang, X.S., Shi, Z.M., 2017. A method for simultaneous estimation of groundwater evapotranspiration and inflow rates in the discharge area using seasonal water table fluctuations. J. Hydrol. 548, 498–507.

Jorenush, M.H., Sepaskhah, A.R., 2003. Modelling capillary rise and soil salinity for shallow saline water table under irrigated and non–irrigated conditions. Agric. Water Manage. 61, 125–141.

Kang, S.Z., Gu, B.J., Du, T., Zhang, J.H., 2003. Crop coeffcient and ratio of transpiration to evapotranspiration of winter wheat and maize in a semi–humid region. Agric. Water Manage. 59, 239–254.

Karimov, A.K., Šimůnek, J., Hanjra, M.A., Avliyakulov, M., Forkutsa, I., 2014. Effects of the shallow water table on water use of winter wheat and ecosystem health: implications for unlocking the potential of groundwater in the Fergana Valley (Central Asia). Agric. Water Manage. 131, 57–69.

Keshavarz, M.R., Vazifedoust, M., Alizadeh, A., 2014. Drought monitoring using a Soil Wetness Deficit Index (SWDI) derived from MODIS satellite data. Agric. Water Manage. 132, 37–45.

Kim, H.W., Hwang, K., Mu, Q.Z., Lee, S.O., Choi, M.H., 2012. Validation of MODIS 16 global terrestrial evapotranspiration products in various climates and land cover types in Asia. KSCE J. Civ. Eng. 16, 229–238.

Kirnak, H., Tas, I., Kaya, C., Higgs, D., 2002. Effects of deficit irrigation on growth, yield, and fruit quality of eggplant under semi–arid conditions. Aust. J. Agric. Res. 53, 1367–1373.

Kisekka, I., Schlegel, A., Ma, L., Gowda, P.H., Prasad, P.V.V., 2017. Optimizing preplant irrigation for maize under limited water in the High Plains. Agric. Water Manage. 187, 154–163.

Kögler, F., Söffker, D., 2017. Water (stress) models and deficit irrigation: System–theoretical description and causality mapping. Ecol. Model. 361, 135–156.

Lee, Y.W., Kim, S.J., 2016. The modified SEBAL for mapping daily spatial evapo-transpiration of South Korea using Three Flux Towers and Terra MODIS Data. Remote Sens. 8. https://doi.org/10.3390/rs8120983.

Li, H.J., Zheng, L., Lei, Y.P., Li, C.Q., Liu, Z.L., Zhang, S.W., 2008. Estimation of water consumption and crop water productivity of winter wheat in North China Plain using remote sensing technology. Agric. Water Manage. 95, 1271–1278.

Liu, Z.Y., Chen, H., Huo, Z.L., Wang, F.X., Shock, C.C., 2016. Analysis of the contribution of groundwater to evapotranspiration in an arid irrigation district with shallow water table. Agric. Water Manage. 171, 131–141.

Luo, Y., Sophocleous, M., 2010. Seasonal groundwater contribution to crop–water use assessed with lysimeter observations and model simulations. J. Hydrol. 389, 325–335.

Ma, S.C., Duan, A.W., Ma, S.T., Yang, S.J., 2016. Effect of early–stage regulated deficit irrigation on stem lodging resistance, leaf photosynthesis, root respiration and yield stability of winter wheat under post–anthesis water stress conditions. Irri. Drain. 65, 673–681.

Man, J.G., Shi, Y., Yu, Z.W., Zhang, Y.L., 2016. Root growth, soil water variation, and grain yield response of winter wheat to supplemental irrigation. Plant. Prod. Sci. 19,

193–205.

McWilliam, J.R., 1986. The national and international importance of drought and salinity effects on agricultural production. Funct. Plant Biol. 13, 1–13.

Miralles, D.G., Holmes, T.R., DeJeu, R.A., Gash, J.H., Meesters, A.G., Dolman, A.J., 2011. Global land–surface evaporation estimated from satellite–based observations. Hrdrol. Earth. Syst. Sci. 15, 453–469.

Mu, Q.Z., Zhao, M.S., Running, S.W., 2011. Improvements to a MODIS global terrestrial evapotranspiration algorithm. Remote Sens. Environ. 115, 1781–1800.

Namuburg, E., Mata–gonzalez, R., Hunter, R.G., Mclendon, T., Martin, D.W., 2005. Phreatophytic vegetation and groundwater fluctuations: A review of current research and application of ecosystem response modeling with an emphasis on great basin vegetation. J. Environ. Manage. 35, 726–740.

Nicolai–Shaw, N., Zscheischler, J., Hirschi, M., Gudmundsson, L., Seneviratne, S., 2017. A drought event composite analysis using satellite remote–sensing based soil moisture. Remote Sens. Environ. 203, 216–225.

Norman, J.M., Kustas, W.P., Humes, K.S., 1995. Source approach for estimating soil and vegetation energy fluxes in observations of directional radiometric surface tem-perature. Agr. For. Meteorol. 77, 263–293.

Panu, U.S., Sharma, T.C., 2002. Challenges in drought research: some perspectives and future directions. Hydrol. Sci. J. Des. Sci. Hydrol. 47, 18–30.

Paul, G., et al., 2014. Investigating the influence of roughness length for heat transport (zoh) on the performance of SEBAL in semi–arid irrigated and dry land agricultural systems. J. Hydrol. 509, 231–244.

Paulson, C.A., 1970. The mathematical representation of wind speed and temperature profiles in the unstable atmospheric surface layer. J. Appl. Meteorol. Clim. 9, 857–861.

Pei, H.W., Min, L.L., Qi, Y.Q., Liu, X.R., Jia, Y.G., Shen, Y.J., Liu, C.M., 2017. Impacts of varied irrigation on field water budegts and crop yields in the North China Plain: Rainfed vs. irrigated double cropping system. Agric. Water Manage. 190, 42–54.

Penman, H.L., 1948. Natural evaporation from open water, bare soil and grass. Proc. R. Soc. Lond. A. Mat. 193, 120–145.

Ramos, T.B., Simionesei, L., Jauch, E., Almeida, C., Neves, R., 2017. Modelling soil water and maize growth dynamics influenced by shallow groundwater conditions in the Sorraia Valley region. Portugal Agric. Water Manage. 185, 27–42.

Ran, H., Kang, S.Z., Li, F.S., Du, T.S., Ding, R.S., Li, S., Tong, L., 2017. Responses of water productivity to irrigation and N supply for hybrid maize seed production in an arid region of Northwest China. J. Arid Land 9, 504–514.

Ren, Z.H., Li, M.Q., Zhang, W.M., 2002. Conversion coefficient of small evaporation pan into E–601B pan in China. J. Appl. Meteor. Sci. 13, 508–512.

Satchithanantham, S., Wilson, H.F., Glenn, A.J., 2017. Contrasting patterns of ground-water evapotranspiration in grass and tree dominated riparian zones of a temperate agricultural catchment. J. Hydrol. 549, 654–666.

Scaini, A., Sánchez, N., Vicente–Serrano, S.M., Martínez–Fernández, J., 2015. SMOS–derived soil moisture anomalies and drought indices: a comparative analysis using in situ measurements. Hydrol. Process. 29, 373–383.

Seneviratne, S.I., Corti, T., Davin, E.L., Hirschi, M., Jaeger, E.B., 2010. Investigating soil moisture–climate interactions in a changing climate: a review. Earth–Sci. Rev. 99, 125–161.

Sepaskhah, A.R., Kanooni, A., Ghasemi, M.M., 2003. Estimating groundwater table con-tributions to corn and sorghum water use. Agric. Water Manage. 58, 67–79.

Sepulcre–Canto, G., Horion, S., Singleton, A., Carrao, H., Vogt, J., 2012. Development of a combined drought indicator to detect agricultural drought in Europe. Nat. Hazard. Earth. Syst. 12, 3519–3531.

Shouse, P.J., Goldberg, S., Skaggs, T.H., Soppe, R.W.O., Ayars, J.E., 2010. Changes in spatial and temporal variability of SAR affected by shallow groundwater manage-ment of an irrigated field. California Agric. Water Manage. 9, 673–680.

Singh, R.K., Irmak, A., Irmak, S., Martin, D.L., 2008. Application of SEBAL model for mapping evapotranspiration and estimating surface energy fluxes in south-central Nebraska. J. Irrig. Drain Eng. 134, 273–285.

Soppe, P.J., Ayars, J.E., 2003. Characterizing ground water use by safflower using weighing lysimeters. Agric. Water Manage. 60, 59–71.

Steinwand, A.L., Harrington, R.F., Or, D., 2006. Water balance for Great Basin phreato-phytes derived from eddy covariance, soil water, and water table measurements. J. Hydrol. 329, 595–605.

Sweet, S.K., Wolfe, D.W., DeGaetano, A., Benner, R., 2017. Anatomy of the 2016 drought in the Northeastern United States: implications for agriculture and water resources in humid climates. Agric. For. Meteorol. 247, 571–581.

Torrion, J.A., Stougaard, R.N., 2017. Impacts and limits of irrigation water management on wheat yield and quality. Crop Sci. 57, 3239–3251.

van Leeuwen, W.J.D., Huete, A.R., Laing, T.W., 1999. MODIS vegetation index compo-siting approach: a prototype with AVHRR data. Remote Sens. Environ. 69, 264–280.

Wang, P., Yu, J., Pozdinakov, S.P., Grinevsky, S.O., Liu, C., 2014a. Shallow groundwater dynamics and its driving forces in extremely arid areas: a case study of the lower Heihe River in northwestern China. Hydrol. Process. 28, 1539–1553.

Wang, X.G., Wang, W., Huang, D., Yong, B., Chen, X., 2014b. Modifying SEBAL model based on the trapezoidal relationship between land surface temperature and vege-tation Index for actual evapotranspiration estimation. Remote. Sens. 6. https://doi.org/10.3390/rs60x000x.

Wang, X.W., Huo, Z.L., Feng, S.Y., Guo, P., Guan, H.D., 2016. Estimating groundwater evapotranspiration from irrigated cropland incorporating root zone soil texture and moisture dynamics. J. Hydrol. 543, 501–509.

Webb, E.K., 1970. Profile relationship: the long–linear range, and extension to strong stability. Q. J. R. Meteorol. Soc. 96, 67–90.

Wu, X.N., Hu, T.S., G, W.X., Jiang, Y., Li, F., 2006. Analysis and study of regional evapotranspiration——Taking Yonglian test area in Hetao Irrigation District for ex-ample. Eng. J. Wuhan Univ. 39, 37–41.

Wu, Y., Shi, X.H., Li, C.Y., Zhao, S.N., Pen, F., Green, T., 2017. Simulation of hydrology and nutrient transport in the Hetao Irrigation District, Inner Mongolia, China. Water. Sui. 9, 169–183.

Wylie, B., 2003. Calibration of remotely sensed, coarse resolution NDVI to CO2 fluxes in a sagebrush–steppe ecosystem. Remote Sens. Environ. 85, 243–255.

Xiong, J., Wu, B.F., Yan, N.N., Zeng, Y., Liu, S.F., 2010. Estimation and validation of land surface evaporation using remote sensing and meteorological data in north China. IEEE J. Sel. Top. Appl. Earth Observ. Remote Sens. 3, 337–344.

Xu, C.Y., Chen, D., 2005. Comparison of seven models for estimation of evapotranspiration and groundwater recharge using lysimeter measurement data in Germany. Hydrol. Process. 19, 3717–3734.

Xu, X., Huang, G.H., Qu, Z.Y., Pereira, L.S., 2010. Assessing the groundwater dynamics and impacts of water saving in the Hetao Irrigation District, Yellow River basin. Agric. Water Manage. 98, 301–313.

Xue, J.Y., Guan, H.D., Huo, Z.L., Wang, F.X., Huang, G.H., Boll, J., 2017. Water saving practices enhance regional efficiency of water consumption and water productivity in an arid agricultural area with shallow groundwater. Agric. Water Manage. 194, 78–89.

Yang, D.W., Sun, F.B., Liu, Z.Y., Cong, Z.T., Lei, Z.D., 2006. Interpreting the complementary relationship in non–humid environments based on the Budyko and Penman hypotheses. Geophys. Res. Lett. 33. https://doi.org/10.1038/s41598–017–18030–5.

Yang, J.F., Wan, S.Q., Deng, W., Zhang, G.X., 2007. Water fluxes at a fluctuating water table and groundwater contributions to wheat water use in the lower Yellow River flood plain. China. Hydrol. Process. 21, 717–724.

Yang, Y.T., Shang, S.H., Jiang, L., 2012. Remote sensing temporal and spatial patterns of evapotranspiration and the responses to water management in a large irrigation district of North China. Agric. For. Meteorol. 164, 112–122.

Yang, G., He, X.L., Li, X.L., Long, A.H., Xue, L.Q., 2017a. Transformation of surface water and groundwater and water balance in the agricultural irrigation area of the Manas River Basin, China. Int. J. Agric. Biol. Eng. 10, 107–118.

Yang, G., Xue, L.Q., He, X.L., Wang, C., Long, A.H., 2017b. Change in land use and evapotranspiration in the Manas River Basin, China with long–term water–saving measures. Sci. Rep. 7. https://doi.org/10.1038/s41598–017–18030–5.

Yang, H.C., Wang, H.X., Fu, G.B., Yan, H.M., Zhao, P.P., 2017c. A modified soil water deficit index (MSWDI) for agricultural drought monitoring: Case study of Songnen Plain. China. Agric. Water Manage. 194, 125–138.

Yang, P., Xia, J., Zhan, C.S., Mo, X.G., Chen, X.J., Hu, S., Chen, J., 2018. Estimation of water consumption for ecosystems based on Vegetation Interfaces Processes Model: A case study of the Aksu River Basin. Northwest China. Sci. Total. Environ. 613–614, 186–195.

Yu, R.H., Liu, T.X., Xu, Y.P., Zhu, C., Zhang, Q., Qu, Z.Y., Liu, X.M., Li, C.Y., 2010. Analysis of salinization dynamics by remote sensing in Hetao Irrigation District of North China. Agric. Water Manage. 97, 1952–1960.

Zdenek, Z., Petr, H., Karel, P., Daniela, S., Jan, B., Miroslave, T., 2017. Impacts of water availability and drought on maize yield–A comparison of 16 indicators. Agric. Water Manage. 188, 126–135.

Zeppel, M., Macinnis, N.C., Palmer, A., Taylor, D., Whiteley, R., Fuentes, S., Yunusa, I., Williams, M., Eamus, D., 2009. An analysis of the sensitivity of sap flux to soil and plant variables assessed for an Australian woodland using a soil–plant–atmosphere model. Funct. Plant Biol. 36 (1120). https://doi.org/10.1071/FP08114_CO.

Zhang, B., Kang, S., Li, F., Zhang, L., 2008. Comparison of three evapotranspiration models to Bowen ratio–energy balance method for a vineyard in an arid desert region of northwest China. Agr. For. Meteorol. 148, 1629–1640.

Zhang, Q., Singh, V.P., Sun, P., Chen, X., Zhang, Z.X., Li, J.F., 2011. Precipitation and stream flow changes in China: changing patterns, causes and implications. J. Hydrol. 410, 204–216.

Zhang, J.P., Tian, H.Y., Guo, B.T., 2012. Determination method of water saving threshold in arid area. Procedia Eng. 28, 873–876.

Zhang, H.Z., Khan, A., Tan, D.K.Y., Luo, H.H., 2017. Rational water and nitrogen management improves root growth, increases yield and maintains water use efficiency of cotton under mulch drip irrigation. Front. Plant Sci. 8. https://doi.org/10.3389/fpls.2017.00912.